Debris-flow monitoring with high-frequency LiDAR scanners: a new method to infer the internal dynamics of debris flows

Jordan Aaron[1,2*], *Raffaele* Spielmann[1,2], *Brian W.* McArdell[1], and *Christoph* Graf[1]

[1] Swiss Federal Institute for Forest, Snow and Landscape Research WSL, 8903 Birmensdorf, Switzerland
[2] Geological Institute, ETH Zürich, 8902 Zürich, Switzerland

Abstract. In-situ measurements of debris-flow properties are crucial for understanding their movement mechanisms and quantifying their impact. Here we present the first results of a field monitoring campaign, at Illgraben, Switzerland, to measure debris-flow parameters using high temporal (10 Hz) and spatial resolution LiDAR sensors at several locations along the channel. The point cloud data is projected onto video images to enhance visualization and aid in the interpretation of the measurements. We process the data using machine vision and deep learning based algorithms, and show that this system can accurately measure front and flow surface velocity, flow depth and bed elevation change, as well as the size, style of motion (e.g. rotating or floating without rotation) and trajectories of individual particles. This system thus provides a promising new method for inferring the internal dynamics of debris flows.

1 Introduction

Improved measurements of in-situ debris-flow properties are critical for better process understanding and risk quantification [1,2]. In particular, high temporal and spatial resolution measurements of critical parameters, including front and surface velocity, flow depth, channel bed elevation change, and individual particle motion are crucial for understanding fundamental debris-flow mechanisms, which include excess pore pressure generation and dissipation, basal and bank erosion, and longitudinal sorting [1-6]. Here we use time-lapse LiDAR scanners, originally developed for autonomous vehicles, combined with image and deep-learning based processing algorithms, to make in-situ measurements of these critical parameters.

Debris-flow properties have been measured in-situ at many locations [1]. These studies have revealed a wealth of information regarding basal forces and pore pressures [3,6], velocity profiles [3], accumulation and depletion volumes between events [7], front and surface velocities [1], as well as flow hydrographs and volumes [1].

LiDAR scanners provide a means to directly measure many in-situ parameters of debris flows [8]. However, this data is difficult to process, and there is a need for algorithms that can be used to derive critical parameters from LiDAR data. Further, high-framerate cameras are capable of collecting a wealth of information about the surface of moving debris flows, but suffer from camera distortion. LiDAR-Camera fusion presents an opportunity to derive 3D information

from these videos, although this has yet to be tested in full scale debris flows.

In the current work we present and analyse a unique dataset of timelapse point clouds of moving debris flows, collected at the Illgraben in Valais, Switzerland. We fuse the point clouds to video data collected at the same site in order to derive high spatial and temporal resolution measurements of critical debris-flow parameters. The results have significant implications for understanding debris-flow motion.

2 Study site and event description

Timelapse point clouds of a moving debris flow were recorded at the Illgraben catchment, located in the Swiss Canton of Valais. The Illgraben has a long history of in-situ monitoring of debris flows [1,6], and a long-term monitoring system was established in the year 2000. Presently, this system includes depth sensors at 5 locations, a force plate that measures basal normal and shear stresses, as well as the LiDAR scanner and video cameras used in the present work.

The Illgraben spans approximately five kilometers from the upper catchment, where debris flows initiate, until the Rhone river, where they deposit. The data used here was collected at a monitoring station approximately 2.5 km from the upper catchment, on a platform suspended over the channel using two cables. The station is located above a concrete check dam, and monitors 60 m upstream and 70 m downstream.

A debris-flow event occurred on September 19, 2021, and was captured by the monitoring system (Fig. 1). This event lasted for approximately 30 minutes, and

---

* Corresponding author: jordan.aaron@erdw.ethz.ch

featured a bouldery front followed by a finer grained slurry. We analysed this event in the present work.

3 Methods

The debris flow was captured using an Ouster OS1-64 (Gen-1) LiDAR scanner that has a 33.2 degree field of view, and 64 scan rings that each collect 2048 points at a frequency of 10 Hz. The scanner is positioned on a platform attached to two cables in the center of the channel. Alongside the LiDAR scanner, two cameras captured the debris flow at a resolution of 1920x1080 pixels, and 25 frames per second. The monitoring station is triggered by an upstream geophone, which sends a signal to a custom logger program which records the LiDAR data.

To take full advantage of the complementary sensors, we adapted the method provided in [9] to estimate the rigid body transformation (translation and rotation) between the two cameras and the LiDAR sensor. The results of this, shown on Fig. 2, allow us to obtain 3D coordinates of pixels in the image, and to colour the point cloud in locations where the field of view overlaps. As described below, this transformation is used to estimate debris-flow front and surface velocities, as well as to track individual particles within the debris flow. Further, we estimated the transformation between the LiDAR data and pre- and post- event DTM's derived from UAV data [7].

We use four methods to estimate debris-flow velocities:

1. Manual mapping of boulders and woody debris in the point cloud data, as described in [13].
2. Particle image velocimetry (PIV) applied to the video frames, with subsequent projection of pixel displacements into the LiDAR point clouds [14].
3. PIV applied to hillshade projections of the LiDAR data [14].
4. Automatic detection and localization of boulders and woody debris using a convolutional neural network [14].

For methods 2 and 3, the Matlab toolbox PIVLab [10] was used.

For method 4, we trained an off-the-shelf implementation of YoloV5 [11] to automatically detect large boulders and woody debris in the video images [14]. Subsequently, we use the 'Sort' algorithm [12] to associate detections in subsequent video frames into tracks of individual particles. Finally, we projected the track detections into the LiDAR point clouds to obtain their 3D position.

We obtained instantaneous flow depths by differencing each frame obtained during the debris-flow event with the pre-event scan, assuming that the channel-bed elevation remains constant. A similar procedure was used to obtain the height difference between pre- and post- event scans, in order to highlight areas of erosion and deposition. There are some substantial uncertainties in this flow-depth estimation procedure, because the true base of the flow is unknown due to erosion and deposition through time during the event.

4 Results and discussion

We captured a continuous time series of point clouds throughout the event, as shown on Fig. 1. This data clearly show the front arrival, the trajectories of boulders and woody debris within the flow, as well as the change in the height of the surface of the debris flow. Manual mapping and the two PIV based velocity estimate methods show that the front velocity varies between 0.8 and 1.75 m/s, and surface velocities during the event reach up to about 3 m/s [13].
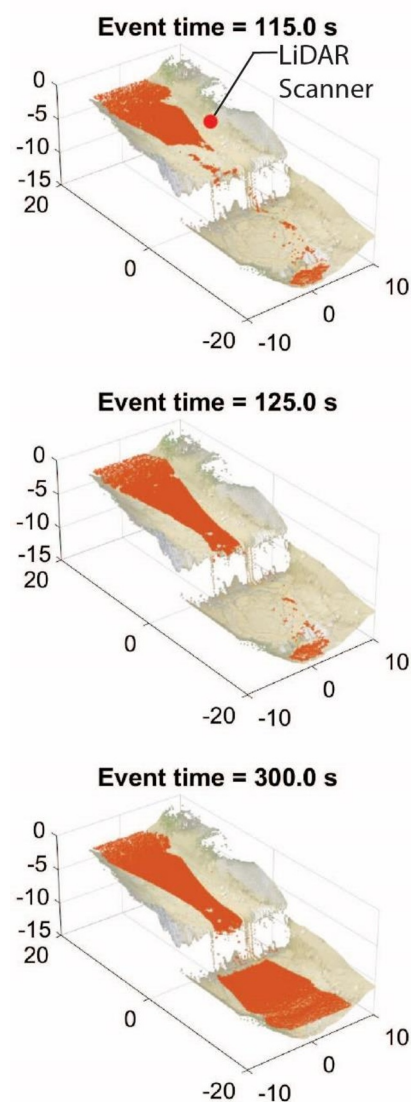

Fig. 1: Overview of sensor setup, arrival of the front and overtopping of the check dam (lower panel). LiDAR data is overlain on a UAV derived DTM of the site (data provided courtesy of T. de Haas using methods described in [7]). Axis ticks are in m, and referenced to a local coordinate system.

Our object detector achieved a test-set precision of ~0.8, and a recall of ~0.6 [14]. The sort algorithm identified about 15,800 tracks, 5,513 of which were present for more than 1 s. The difference between these two values indicates that the same track is likely detected multiple times by the algorithm. A more robust association of detections into tracks is a subject for future work. Example detections from the network are shown Fig. 2, as are the corresponding point clouds for select features. Velocities of certain features are shown

on Fig. 3. As can be seen on the right of Fig. 2, the two detections near the camera are precise, however image distortion further from the camera results in the extraction of points behind the target feature. Further processing of the extracted features should overcome this limitation.
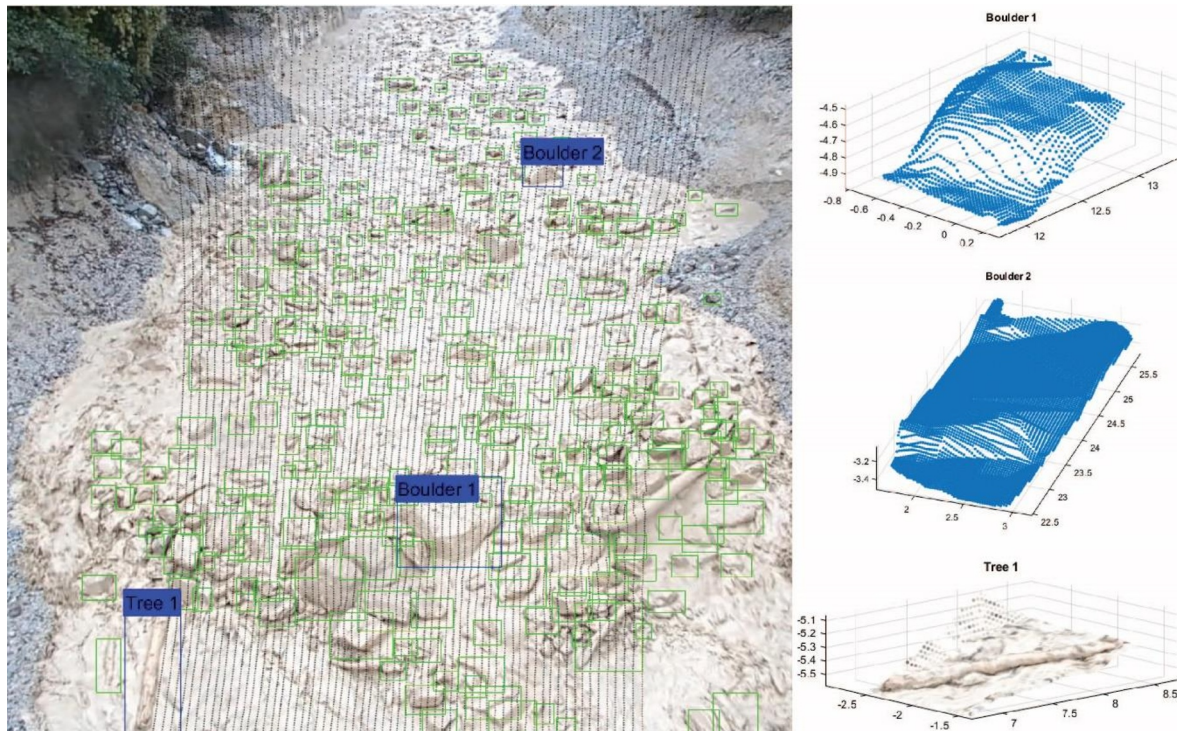
Fig. 2: Object detector output for a frame corresponding to the front arrival. The blue rectangle show the neural network detections, the black dots show the LiDAR point cloud projected onto the image, and the red boxes show three features whose corresponding point cloud was extracted, and are shown on the right side of the Figure. The features were extracted following interpolation of the point cloud, and the tree is colored based on the camera image. The units of the ticks on the inset are in meters, and are referenced to a local coordinate system.
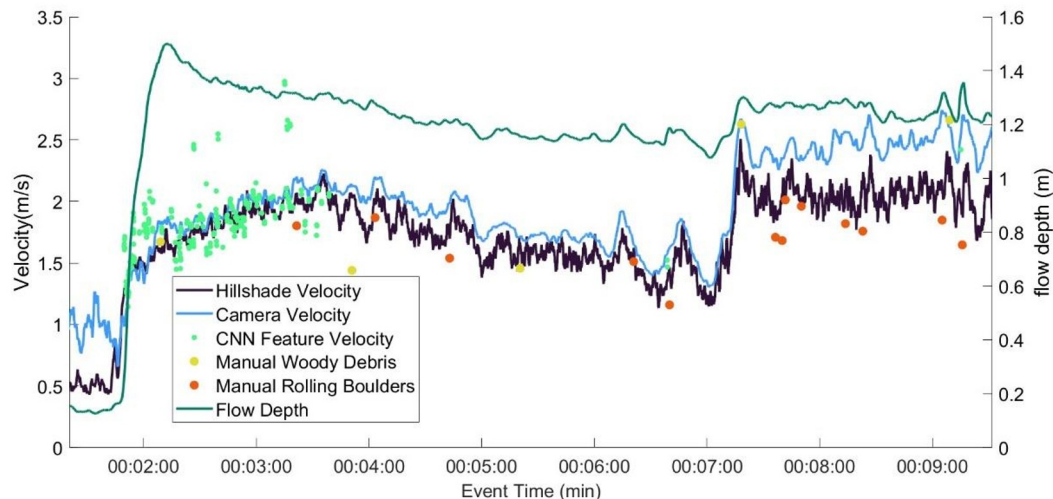

Fig. 3: Surface velocity through time, estimated using the methods described in [14] and in the text.

We find that surface velocities of the event vary strongly (Fig. 3), likely due to changing composition of the flow through time. We note a distinct increase in velocity at approximately 7 minutes (Fig. 3). Interestingly, our two PIV-based automatic velocity estimation techniques provide different velocity estimates following this jump (see also [14]). Manual feature mapping indicates that different objects have different velocities (Fig 3). The two automatic methods appear to be sensitive to different features of the flow [14].

Finally, the vertical difference between the pre- and post- event scans (Fig. 4) show net deposition above the check dam (y-coordinate > 0), and some erosion downstream of the check dam where the channel goes around a bend. We note that the LiDAR scan does not span the width of the channel at all locations, so this

accumulation/depletion estimate is only valid for a subset of this particular location.
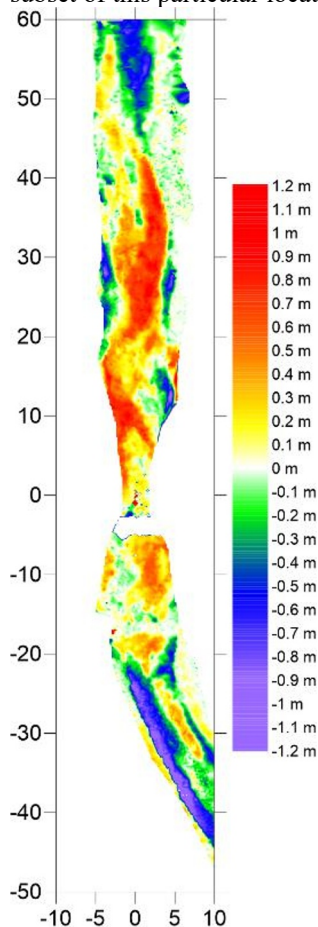
Fig. 4: Erosion and deposition areas obtained from differencing the pre- and post- event scans. The coordinate system is an unreferenced local coordinate system, with tick values in meters.

5 Conclusion and outlook

Timelapse LiDAR scanners, fused with high framerate camera data, provides a means for collecting a wealth of data from moving debris flows. Here we have shown that this information can be used to automatically derive dense surface velocity, flow depth, bed elevation change and feature trajectory information. These parameters are crucial for understanding debris-flow mechanisms, and ultimately managing their hazard.

The results presented herein were taken from the first event captured with the system at Illgraben. Over the next years, further events that occur in the catchment will enable an analysis of a variety of relevant debris-flow phenomena, such as the temporal and spatial variation in the size of large features, superelevation, and surge velocity, which will help to elucidate some of the processes described here. Further, the influence of debris-flow velocity and feature size will be explored in future events. It is expected that careful analysis of this data will reveal surprising features of debris-flow motion, and will provide a foundation for a new understanding of these destructive flows.

6 References

1. M. Hürlimann, V. Coviello, C. Bel, X. Guo, M. Berti, C. Graf, J. Hübl, S. Miyata, J. Smith, and H. Y. Yin (2019). Earth-Science Reviews, 199, 102981
2. O. Hungr (2000) Earth Surf. Process. Landforms, 25: 483-495.
3. G. Nagl, J. Hübl, and R. Kaitna (2020) Earth Surf. Process. Landforms, 45: 1764– 1776
4. O. Hungr, S. Leroueil, and L. Picarelli (2014) Landslides, vol. 11, no. 2
5. C.G. Johnson, B. P. Kokelaar, R. M. Iverson, M. Logan, R. G. LaHusen, and J. M. N. T. Gray (2012), J. Geophys. Res., 117
6. B. W. McArdell, P. Bartelt, and J. Kowalski (2007) Geophys. Res. Lett., 34, L07406
7. T. de Haas, B. W. McArdell, W. Nijland, A.S. Åberg, J. Hirschberg, and P. Huguenin (2022) Geophysical Research Letters, p.e2021GL097611
8. F. K. Rengers, T.D. Rapstine, M. Olsen, K. E. Allstadt, R. M. Iverson, B. Leshchinsky, M. Obryk, J. B. Smith (2021) Environmental & Engineering Geoscience 27 (1): 113–126
9. J.K. Huang, and J. W. Grizzle (2020) IEEE Access, vol. 8, pp. 134101-134110, 2020
10. W. Thielicke, R. Sonntag (2021) Journal of Open Research Software, 9: 12
11. Redmon, J., Divvala, S., Girshick, R., & Farhadi, A. IEEE Conference on Computer Vision and Pattern Recognition (CVPR), 2016
12. Bewley, Z. Ge, L. Ott, F. Ramos and B. Upcroft, (2016) IEEE International Conference on Image Processing (ICIP), 2016, pp. 3464-3468
13. R. Spielmann, J. Aaron, B. W. McArdell, (2023) 8th International Conference on Debris Flow Hazard Mitigation, DFHM8, 26-29 June 2023, Torino, Italy
14. J. Aaron, R. Spielmann, B. W. McArdell, C. Graf, Geophysical Research Letters, 50, e2022GL102373 (2023)